Journal of Materials Chemistry A

PAPER

View Article Online
View Journal | View Issue

Cite this: *J. Mater. Chem. A*, 2014, **2**, 2648

Electrochemical synthesis of coaxial TiO_2–Ag nanowires and their application in photocatalytic water splitting

A. Wouter Maijenburg,[a] Janneke Veerbeek,[a] Roy de Putter,[a] Sjoerd A. Veldhuis,[a] Michel G. C. Zoontjes,[b] Guido Mul,[b] Josep M. Montero-Moreno,[c] Kornelius Nielsch,[c] Helmut Schäfer,[d] Martin Steinhart[d] and Johan E. ten Elshof*[a]

Received 6th November 2013
Accepted 4th December 2013

DOI: 10.1039/c3ta14551d

www.rsc.org/MaterialsA

A new method for the formation of coaxial TiO_2–Ag nanowires is presented, in which TiO_2 nanotubes were formed by the templated electrochemically induced sol–gel method, followed by thermal annealing. The as-formed TiO_2 nanotubes have been successfully filled with a Ag core using a subsequent electrodeposition step. Coaxial nanowires have a very suitable architecture for photocatalysis, solar cells or batteries due to the high contact area between the two different phases, the large outer surface area exposed to the reactant, and short electron diffusion paths. The coaxial nanowires showed a higher efficiency than empty TiO_2 nanotubes and TiO_2 nanotubes with attached Ag nanoparticles in photocatalytic water splitting. Coaxial TiO_2–Ag nanowires formed H_2 at a rate of $\sim 1.23 \times 10^{-3} \pm 0.3 \times 10^{-3}$ mol g^{-1} h^{-1} without deactivation for at least 6 h.

Introduction

One-dimensional nanostructures, such as nanowires and nanotubes, have attracted increasing attention in the last few years. The unique physical and chemical properties of these nanostructures make them promising building blocks for various kinds of future applications, such as nanosensors,[2–4] cell trackers,[5–7] and self-propelling nanomotors.[8–10] Because of their very high surface-to-volume ratio, some of the most interesting applications of nanowires and nanotubes are in solar cells and photocatalytic water splitting.[1,11–13] The physical properties of most semiconductors demand the use of one-dimensional nanostructures, since the diffusion length of minority charge carriers in most semiconductors is of the order of 100 nm, while the absorption depth near the bandgap is of the order of 10 μm.[16–19] In this respect, a maximum of solar light can be absorbed over the nanowire length, while the nanowire diameter is small enough for efficient electron and hole diffusion, thereby leading to high efficiency.[20]

With a band gap of 3.0 eV, high chemical stability and low synthesis costs, TiO_2 in the anatase phase is a very interesting material for efficient solar hydrogen formation.[20–22] TiO_2 is therefore the most commonly used material for photocatalytic water splitting and solar cells.[23–25] TiO_2 nanotubes are also often used for photocatalytic water splitting,[14,15,26–30] although few authors present actual H_2 formation rates.[14,15,29] Alternatively, TiO_2 nanowires and nanotubes can also be used as micromotors, microfireworks or micropumps upon excitation by UV light,[31] as catalysts for methanol (electro)oxidation[32,33] or as anode materials in Li-ion batteries.[34–36] The formation of a core–shell structure based on TiO_2 nanotubes may also be advantageous for such applications.

TiO_2 nanowires and nanotubes can be formed *via* several techniques, *i.e.* hydrothermal treatment,[37] anodization of titanium foils,[38–40] atomic layer deposition (ALD),[41,42] modified sol–gel route,[11,43,44] sol–gel electrophoresis,[45,46] electrochemical deposition,[47,48] and electrochemically induced sol–gel synthesis.[49,50] As sol–gel electrophoresis and the modified sol–gel route provide nanowires or nanotubes consisting of smaller sol–gel particles, the resulting nanostructures are very brittle with rough surfaces, which decreases the mechanical stability of the formed nanowires. Although a large area of single crystalline TiO_2 nanotubes with tuneable dimensions can be made by anodization of Ti foil, the main disadvantage of this technique is that the formed nanotubes do not contain a conductive back electrode, so that extra steps need to be applied before these nanotubes can be filled with a second material.[51] In contrast, the availability of a back electrode and the synthesis of smooth films or nanostructures make the electrochemically induced sol–gel method a very promising technique for the synthesis of core–shell nanostructures with a TiO_2 shell.

[a]*Inorganic Materials Science, MESA+ Institute for Nanotechnology, University of Twente, P.O. Box 217, 7500 AE Enschede, The Netherlands. E-mail: j.e.tenelshof@utwente.nl*

[b]*Photocatalytic Synthesis, MESA+ Institute for Nanotechnology, University of Twente, P.O. Box 217, 7500 AE Enschede, The Netherlands*

[c]*Multifunctional Nanostructures, Institute of Applied Physics, University of Hamburg, Jungiusstrasse 11, 20355 Hamburg, Germany*

[d]*Physikalische Chemie, Institut für Chemie neuer Materialien, Universität Osnabrück, Barbarastr. 7, D-49069 Osnabrück, Germany*

The electrochemically induced sol–gel method for the cathodic electrodeposition of titanium dioxide thin films was first introduced by Natarajan and Nogami[52] and was further improved by Karuppuchamy *et al.*[53,54] This method involves dissolving titanium oxysulfate ($TiOSO_4$) powder in an aqueous solution of hydrogen peroxide (H_2O_2), yielding a peroxotitanate complex ($Ti(O_2)SO_4$) (eqn (1)):

$$TiOSO_4 + H_2O_2 \rightarrow Ti(O_2)SO_4 + H_2O. \quad (1)$$

At potentials more negative than −0.9 V *vs.* Ag/AgCl, nitrate is reduced to form hydroxyl ions (eqn (2)),[54] and consequently the pH in the vicinity of the electrode surface is increased:[49]

$$NO_3^- + H_2O + 2e^- \rightarrow NO_2^- + 2OH^-. \quad (2)$$

This local increase in pH is necessary for the formation of a titanium hydroxide gel as shown in eqn (3):[54]

$$Ti(O_2)SO_4 + 2OH^- + (x+1)H_2O \rightarrow TiO(OH)_2\cdot xH_2O + H_2O_2 + SO_4^{2-}. \quad (3)$$

According to differential thermal analysis data of Natarajan and Nogami, water is removed from the gel during thermal annealing around 283 °C (eqn (4)), resulting in an amorphous TiO_2 phase.[52] When the temperature is increased above 365 °C, crystallization into the anatase phase occurs:[52,55]

$$TiO(OH)_2\cdot xH_2O \rightarrow TiO_2 + (x+1)H_2O. \quad (4)$$

By employing the electrochemically induced sol–gel method within the pores of an anodic aluminium oxide (AAO) template, nanowires and nanotubes can be formed. Nanowires were previously made using templates with pores of 50 nm diameter and smaller.[49,50] In the present study, AAO templates with a diameter of 200 nm were used, which resulted in nanotube formation. The mechanism of nanotube formation was previously described by Maas *et al.*, and occurs by removal of water from the titanium hydroxide gel.[56] The first 6 steps in Fig. 1 provide a schematic representation of TiO_2 nanotube formation according to the above reactions.

As mentioned above, an advantage of the electrochemically induced sol–gel method for TiO_2 nanotube formation is the availability of a cathode at one end of the AAO membrane or template. This allows for the formation of coaxial nanowires by filling the TiO_2 nanotubes in a subsequent deposition step with a second phase like silver (step 7 in Fig. 1). By combining an n-type semiconductor like TiO_2 with a noble metal, a Schottky barrier is formed when the work function of the metal is smaller than that of the n-type semiconductor, which diminishes electron–hole recombination.[20] This is schematically depicted in Fig. 2. Upon illumination, electrons and holes are formed in the TiO_2 shell layer (step 1). As the electrons are transferred to the silver core of the wires, the holes go to the surface of the TiO_2 phase (steps 2), where they are known to react with water to form H^+ ions and O_2 (steps 3). In the Ag phase, at the outer ends of the coaxial nanowire, electrons and protons can combine to form H_2 (step 4).[20–22]

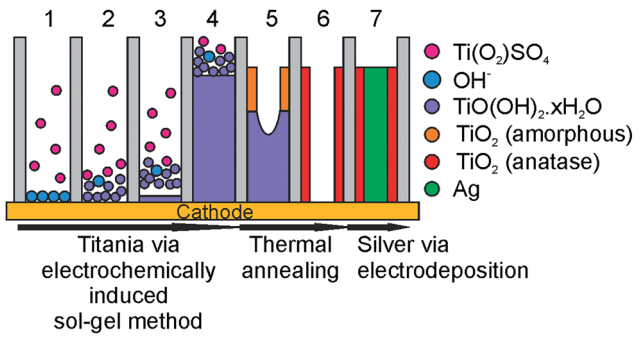

Fig. 1 Schematic overview of the preparation of coaxial TiO_2–Ag nanowires using the electrochemically induced sol–gel method: formation of OH^- at the electrode (step 1, reaction (2)), reaction of $Ti(O_2)SO_4$ with OH^- to form $TiO(OH)_2\cdot xH_2O$ and filling of the template (steps 2–4, reaction (3)), drying and thermal annealing of the titanium hydroxide gel to TiO_2 (steps 5–6, reaction (4)), and filling of the TiO_2 nanotubes with Ag (step 7).

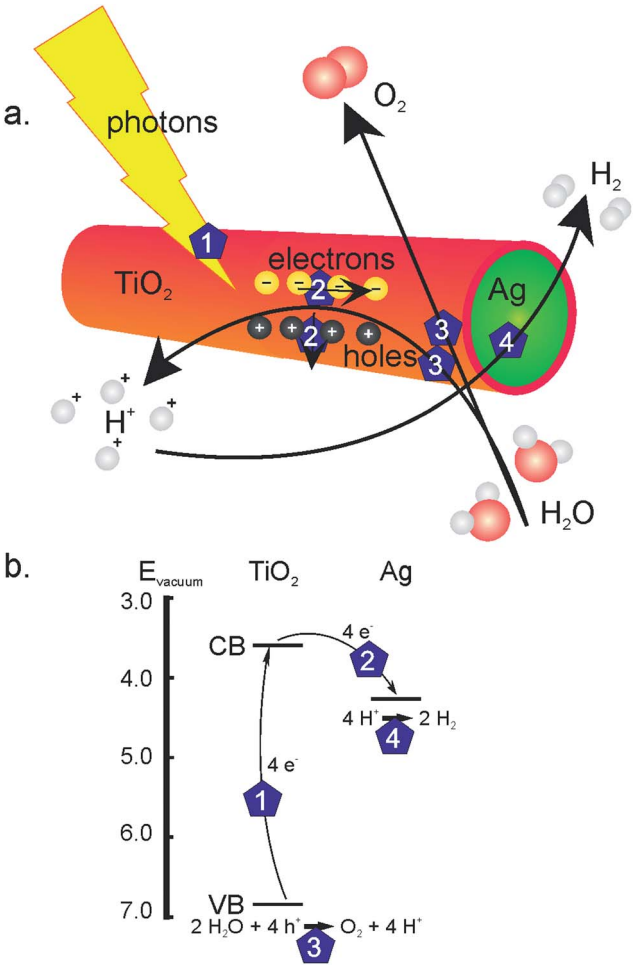

Fig. 2 (a) Schematic representation and (b) band energy diagram of water splitting by coaxial TiO_2–Ag nanowires in an alkaline solution: formation of electrons and holes in the TiO_2 phase (step 1), electron–hole separation at the TiO_2–Ag interface (steps 2), water oxidation at the TiO_2 surface (steps 3) and H_2 formation at the Ag surface (step 4).

In this study, we employed the electrochemically induced sol–gel method for the formation of TiO_2 nanotubes and filled these nanotubes with a silver phase using electrodeposition. The photocatalytic activity of the coaxial TiO_2–Ag nanowires in splitting water was investigated in an alkaline solution. Furthermore, the photocatalytic activity of the coaxial TiO_2–Ag nanowires was compared with similar TiO_2 nanostructures with/without Ag that were also prepared in this study, and with values reported in other studies.

Results and discussion

Since it was found that annealing within a template resulted in crystallization at a higher temperature than in films, we investigated the crystallinity of different samples annealed at variable temperatures (Fig. 3). The figure shows that TiO_2 within an AAO template crystallized into a mixture of anatase, rutile and brookite between 525 °C and 550 °C, while an unconstrained TiO_2 gel made *via* the same procedure crystallized below 400 °C (data not shown, see *e.g.* Natarajan and Nogami).[52] Also for TiO_2 powder made *via* a different sol–gel process, it is known that TiO_2 crystallizes below 400 °C.[57] A possible explanation for the large difference found in crystallization temperatures between TiO_2 powder and the nanotubes formed in this study may be clamping of the TiO_2 phase on the sidewalls of the AAO template. Clamping was also previously found to retard the crystallization of $BaTiO_3$ and $SrRuO_3$ films.[58]

After annealing the titania gel inside an AAO membrane for 2 h at 650 °C, the TiO_2 gel was crystallized into a polycrystalline mixture of anatase, rutile and brookite polymorphs of TiO_2, with no preferred orientation. It is noted that the presence of all three polymorphs of TiO_2 is known to have a positive influence on the photocatalytic activity as previously discussed in several other studies.[59,60] After annealing at 550 °C, the formation of an unidentified impurity phase was observed, which is denoted with an asterisk. For the TiO_2 nanotubes, crystallite sizes of approximately 42 and 45 nm were found when annealed at 550 and 650 °C, respectively, showing negligible crystallite growth. For TiO_2 films made *via* the same method we observed exponential crystallite growth with sizes of 19 and 28 nm when annealed at 550 and 650 °C, respectively.

The cross-section of a membrane containing TiO_2 nanotubes after annealing at 650 °C shows a gradual decrease in thickness of the TiO_2 coating on the AAO pore walls from ~55 nm at the

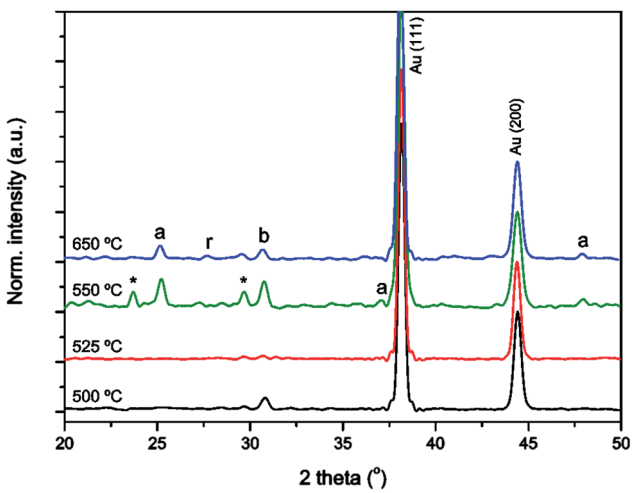

Fig. 3 XRD patterns of TiO_2 nanotubes annealed for 2 h at 500 °C (black line), 525 °C (red line), 550 °C (green line), and 650 °C (blue line), with the tubes still inside an AAO membrane; diffraction peaks were assigned to Au (PDF # 00-004-0784), anatase TiO_2 (a, PDF # 00-021-1272), rutile TiO_2 (r, PDF # 00-021-1276) and brookite TiO_2 (b, PDF # 00-029-1360); an unknown impurity phase is denoted with an asterisk (*).

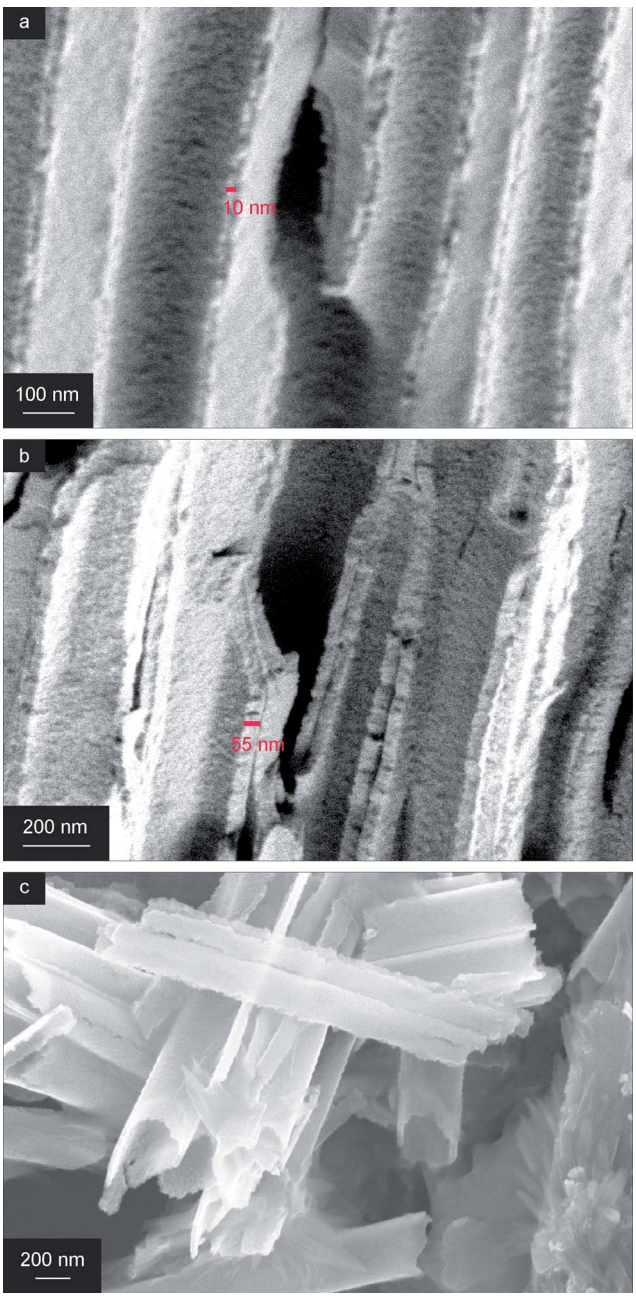

Fig. 4 Cross-sectional SEM images of TiO_2 nanotubes inside the membrane: (a) at the top of the membrane, (b) at the bottom of the membrane, and (c) TiO_2 nanotubes after dissolving the membrane.

bottom of the membrane (Fig. 4b), which is the cathode side, to ~10 nm at the top of the membrane (Fig. 4a). The thickness gradient can be explained by the formation of a thicker gel near the electrode as OH^- is formed here. To put the thickness of the TiO_2 phase into the perspective of the proposed application in solar water splitting, a wall thickness less than 20 nm would provide efficient charge carrier separation as the minority carrier diffusion length in TiO_2 is approximately 20 nm.[61] This means that the most efficient charge carrier separation takes place only in the upper part of these nanotubes. On the other hand, the chance that a photon is absorbed by the material is higher when the titania wall is thicker. It is expected that a lower concentration of KNO_3 in the electrolyte solution can provide TiO_2 nanotubes with thinner walls, but a trade-off has to be made between carrier diffusion length, mechanical stability of the nanotubes and degree of photon absorption. After dissolving the membrane, a droplet of nanotube solution was placed on a silicon wafer for visualization with SEM. These nanotubes appear to be smooth at first sight, but a closer look reveals that they are composed of very small grains (Fig. 4c).

After the formation of a titania gel inside the AAO membrane, a fraction of the samples was dried overnight at 100 °C to remove water, while the other fraction was annealed for 2 h at 650 °C to form crystalline nanotubes. When silver was deposited inside a membrane after drying at 100 °C, TiO_2 nanotubes containing isolated Ag nanoparticles (TiO_2–Ag nanotubes) were formed after Ag electrodeposition and subsequent annealing (Fig. 5a). The reason for this is that the Ag^+ ions could penetrate the gel, because the titania phase was not completely dense after exposure to 100 °C. As a result, Ag nuclei formed where such ions combined with an electron. During subsequent heat treatment at 650 °C, these Ag nanoparticles were transported to the pore walls along with the collapse of the titania gel.

However, when Ag was electrodeposited after high temperature annealing of the TiO_2 gel at 650 °C, solid TiO_2 nanotubes formed first, and dense silver nanowires were deposited inside these tubes. This resulted in the formation of coaxial TiO_2–Ag nanowires (Fig. 5b and 6).

The TEM image of a TiO_2 nanotube with a Ag core is shown in Fig. 6a. Especially the Electron Energy Loss Spectroscopy (EELS) TEM map in Fig. 6b clearly shows the architecture of the core–shell structure, with a higher concentration of Ti (red) at the outside of the coaxial nanowire, and a higher concentration of Ag (green) at the interior of the tube.

The photocatalytic activities in photocatalytic water splitting of coaxial TiO_2–Ag nanowires, empty TiO_2 nanotubes and TiO_2–Ag nanotubes with isolated Ag nanoparticles are compared in Fig. 7a after 3.5 h of irradiation. The coaxial TiO_2–Ag nanowires formed significantly more H_2 than the TiO_2 nanotubes and the TiO_2–Ag nanotubes. H_2 formation was absent in the reference reactor containing aqueous 1 M NaOH solution. Only the intensity of the H_2 signals from the coaxial TiO_2–Ag nanowires was sufficient for automatic integration, so for this system a long-term measurement was performed (Fig. 7b). Continuous H_2 formation was observed for a period of 6 h at a rate of $6.2 \pm 1.5 \times 10^{-6}$ mol h^{-1}, after which the reaction was terminated.

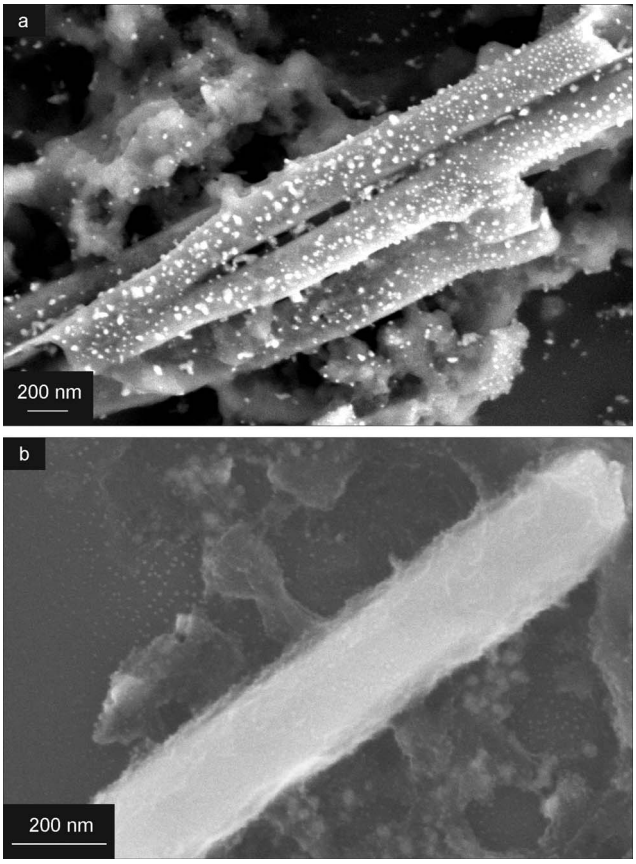

Fig. 5 SEM images of (a) TiO_2–Ag nanotubes from a two step electrodeposition process with an intermediate TiO_2 gel drying at 100 °C, and (b) a coaxial TiO_2–Ag nanowire from a two step electrodeposition process with intermediate TiO_2 tube solidification at 650 °C. See the main text for details.

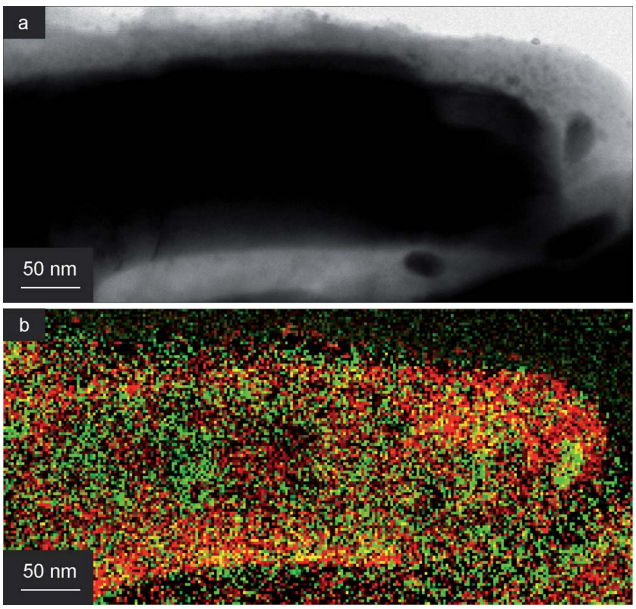

Fig. 6 (a) TEM image and (b) EELS TEM map of a TiO_2 nanotube (red) filled with Ag (green).

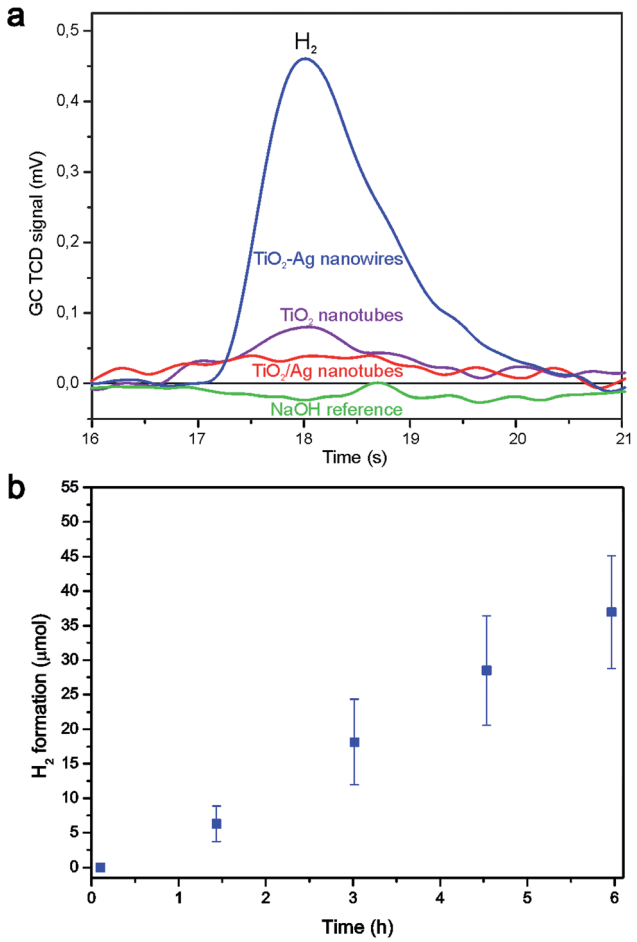

Fig. 7 (a) GC TCD peaks showing H_2 formation from TiO_2 nanotubes (purple line), TiO_2/Ag nanotubes (red line), TiO_2–Ag nanowires (blue line) and NaOH baseline (green line). (b) Moles of H_2 formed from coaxial TiO_2–Ag nanowires during 6 h measurement in 1 M NaOH.

Several possible explanations can be given for the higher H_2 formation rate by the coaxial TiO_2–Ag nanowires compared to the TiO_2 nanotubes: (1) the availability of an H_2 evolution catalyst such as Ag, which decreases the chance for electron–hole recombination, (2) the use of the metallic Ag core as a mirror to reflect photons back into the TiO_2 shell, which could approximately double the number of photons captured by the photocatalyst, and/or (3) the use of the Ag core for enhancement of the light absorption due to localized surface plasmon resonance of the Ag nanowire.

Comparing the TiO_2/Ag nanotubes with the coaxial nanowires, several possible explanations can be given for the higher H_2 formation rate of the latter: (1) the availability of a larger amount of Ag catalyst with an increased interface between the photocatalyst and H_2 evolution catalyst, which shortens the electron diffusion length and decreases the chance for electron–hole recombination in the coaxial nanowires, and/or (2) since most of the Ag particles are located at the outside of the TiO_2 nanotubes, these particles may prevent some of the photons from reaching the TiO_2 phase which decreases the efficiency of this system. It is however unlikely that the second possibility alone can explain the large difference.

For comparison with other data from the literature, the observed H_2 formation rate was corrected for either the weight of nanowires that was put in solution or the initial surface area of the template, resulting in an H_2 formation rate of $1.2 \times 10^{-3} \pm 0.3 \times 10^{-3}$ mol g^{-1} h^{-1} and $0.18 \times 10^{-6} \pm 0.04 \times 10^{-6}$ mol cm^{-2} h^{-1}, respectively. As can be seen from Table 1, this was higher than what we measured previously using segmented ZnO|Ag nanowires, where H_2 formation at a rate of 6.9×10^{-6} mol g^{-1} h^{-1} was observed.[1] Especially the increased surface area between the photocatalytic oxide phase and the H_2 evolution catalyst, and the shorter diffusion length for electrons to cross the oxide–metal junction are likely explanations for the difference of ~3 orders of magnitude. Obviously, the use of different photocatalytic materials and the fact that methanol was used as the hole scavenger by the ZnO|Ag nanowires also influence the efficiency.

We also compared the H_2 formation rate from the coaxial TiO_2–Ag nanowires with an alternative coaxial TiO_2–Ag nanowire system in which the TiO_2 phase was prepared by Atomic Layer Deposition (ALD), and the Ag phase by electrodeposition. The SEM image of TiO_2 nanotubes made by ALD is shown in Fig. 8. Compared to the SEM image in Fig. 4c, the nanotubes made by both techniques have approximately the same dimensions, but the nanotubes made by ALD appear much smoother. It was confirmed by XRD that the TiO_2 nanotubes made by ALD are also polycrystalline without preferred orientation, the difference being that they are composed of large anatase crystallites with a size of 250–300 nm as shown in ref. 62. Using the same setup for photocatalytic water splitting, we found a H_2 formation rate of 0.26×10^{-3} mol g^{-1} h^{-1} for the ALD-based system, which is ~4.7 times lower than the rate found for the electrochemically deposited TiO_2–Ag system and also lower than the TiO_2 nanotubes without Ag. Since the TiO_2 nanotubes deposited by ALD were polycrystalline anatase with a larger crystallite size, it was expected *a priori* that the photocatalytic activity of these nanowires would be higher, since the concentration of grain boundaries that can enhance undesired electron–hole recombination is lower. On the other hand, it is known that photocatalytic water splitting is more efficient on specific facets, so when these facets are not exposed to the solution this will lead to a lower H_2 evolution rate. Of course, the different TiO_2 polymorphs that were observed in both systems, purely anatase for the ALD-based system *vs.* a mixture of anatase, rutile and brookite for the system prepared *via* the electrochemically induced sol–gel method, might also influence the photocatalytic activity. Also other effects like impurities or secondary phases can have a positive effect on the photocatalytic properties of the electrochemically synthesized system. As listed in Table 1, there are also some other minor differences between the two systems in nanowire length, diameter and TiO_2 shell thickness, but it is not expected that these differences alone can explain the large difference in photocatalytic activity.

Only a few other publications report H_2 evolution from TiO_2 nanotubes, and these are listed in Table 1. The geometries and process conditions vary widely between these studies, so that direct comparison of these data should be done with care. Besides one other publication on hydrogen evolution by

Table 1 Comparison of H_2 formation from different nanowire and nanotube systems

Nanowire/tube system	Ref.	H_2 formation mol g^{-1} h^{-1}	H_2 formation mol cm^{-2} h^{-1}	Dimensions diameter (TiO_2 thickness) × length	Electrolyte	Light source
Coaxial TiO_2–Ag nanowires	This work	1.2×10^{-3}	0.18×10^{-6}	200 nm (10–50 nm) × 40 μm	1.0 M NaOH	10 W Hg lamp
Coaxial TiO_2–Ag nanowires by ALD	This work	0.26×10^{-3}		175 nm (20 nm) × 8 μm	1.0 M NaOH	10 W Hg lamp
Segmented Ag|ZnO nanowires	1	6.9×10^{-6}		200 nm × 6 μm	4 : 1 v/v MeOH/H_2O	60 W Hg lamp
Anodized TiO_2 with Pt mesh counter electrode	14	2.83×10^{-3}		60 nm (10 nm) × 1.5 μm	0.01 M KOH, 1.0 mM KI	400 W Hg lamp
Anodized TiO_2 with Pt counter electrode in the second compartment	15		97×10^{-6}	75 nm (20–70 nm) × 6 μm	1.0 M KOH	350 W Xe lamp
Anodized TiO_2 containing evaporated Pt	29		14×10^{-6}	150 nm (30 nm) × 650 nm	0.01 M KOH, 1.0 mM KI	400 W metal hydride lamp

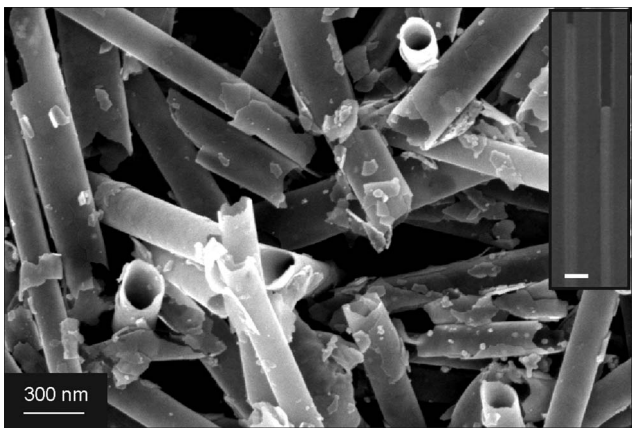

Fig. 8 SEM image of TiO_2 nanotubes made by ALD before Ag filling, after release from the template. The inset shows coaxial TiO_2–Ag nanowires inside the membrane, where the TiO_2 phase is visible as a bright white phase covering the pore walls at the top of the figure, and the Ag phase is visible as a solid nanowire at the bottom of the figure.

autonomous nanowires in methanol,[1] all other studies involve photoelectrochemical cells with compositionally distinct, and in some cases spatially separated, hydrogen and oxygen evolution catalysts. Only one publication reports the H_2 evolution rate per weight of used material for TiO_2 nanotubes, resulting in an evolution rate of 2.83×10^{-3} mol g^{-1} h^{-1} H_2.[14] This is a factor of 2.3 higher than our current result, and it might be explained by the difference in crystallinity of TiO_2, as anodization can result in the formation of single crystalline TiO_2 nanotubes, while polycrystalline TiO_2 nanotubes were made in the current research. Two other main differences are that a light source with higher energy is used in ref. 14, and that an IO_3^-/I^- redox couple was used as a redox mediator to prevent the recombination of H_2 and O_2 into H_2O. Both these differences also drastically influence the H_2 evolution rate.

Others calculated the H_2 formation rate per unit surface area of the anodized Ti foil, resulting in H_2 formation rates of 97×10^{-6} mol cm^{-2} h^{-1},[15] and 14×10^{-6} mol cm^{-2} h^{-1},[29] which are both much higher than our current result using coaxial TiO_2–Ag nanowires made *via* the electrochemically induced sol–gel method. Part of this difference may be explained by the different methods used to measure the surface area: the surface area of the AAO template before dissolution *vs.* the anodized surface area of the Ti foil. Both authors used Pt as a counter electrode[15] or as a thin layer on top of the nanotubes for enhanced photocatalytic activity.[29] Also here a light source with higher energy was used in both studies and an IO_3^-/I^- redox couple was used as a redox mediator in one of the two studies to prevent the recombination of H_2 and O_2 into H_2O.[29] Another method to prevent the recombination of H_2 and O_2 is to split the electrodes in a two-compartment setup.[15] On the other hand, even though efficiencies could be increased by preventing H_2 and O_2 recombination, we have shown that coaxial TiO_2–Ag nanowires are able to split water autonomously without addition of sacrificial agents, redox mediators or external power supply. This can be of advantage for self-fuelling nanodevices in aqueous environments or to generate H_2 at a specific location.

Next to the possible explanation of different crystallinity, the use of redox mediators and two-compartment setups, it is still difficult to directly compare these results, because every author uses different light sources and electrolytes that both have a large impact on the efficiency for H_2 formation. In that respect, a better way for comparison would be to keep the nanowires attached to the substrate for photocurrent measurements. Also the applied potential should be compensated for the reference electrode and pH of the solution, as illustrated by Seabold and Choi.[63] Unfortunately, with the AAO templates available for this study, it was not possible to keep the nanotubes or nanowires standing on the substrate after dissolving the template because the nanowire/nanotube connection to the bottom was mechanically too weak. Additionally, standardized simulated AM1.5 solar illumination with an energy of 100 mW cm^{-2} should be used in all measurements, but unfortunately these solar simulators are expensive and not available in every lab.

Several strategies can be pursued to further improve the activity and H_2 formation rate. One of these strategies includes changing the alkaline electrolyte for water splitting to either an acidic or neutral electrolyte.[30] The second method includes the use of a sacrificial agent, *e.g.* methanol, or a redox mediator, *e.g.* KI, to increase the H_2 formation rate.[26,64–66] As a third option, the

activity for water splitting can be improved by adding an oxidation catalyst, *e.g.* Mn_3O_4, for more efficient O_2 formation. In the fourth method, the dimensions of the coaxial TiO_2–Ag nanowires could be changed in order to find an optimum in total diameter, TiO_2 shell thickness and nanowire length. These methods should be systematically investigated in future research.

Experimental

All chemicals were purchased from commercial sources and used without further purification. Titanium oxysulfate ($TiOSO_4$, synthesis grade), hydrogen peroxide (H_2O_2, 35 wt%), boric acid (H_3BO_3, purity 99.97%), sodium hydroxide (NaOH, purity >98%) and titanium(IV) isopropoxide (99%) were purchased from Sigma-Aldrich. Silver nitrate ($AgNO_3$, purity >99%), nitric acid (HNO_3, 65%), potassium nitrate (KNO_3, purity >99%), chromium(VI) oxide (CrO_3, purity 99.5%) and phosphoric acid (H_3PO_4, >85%) were purchased from Acros Organics. Oxalic acid ($C_2H_2O_4$, p.a. grade) was purchased from Merck Millipore. Silver sulfate (Ag_2SO_4, purity 99.999%), diammonium citrate (purity >99%) and potassium thiocyanide (KSCN, purity 98%) were purchased from Alfa Aesar. Milli-Q water with a resistivity of 18.2 MΩ cm was used in all experiments.

Anodized aluminium oxide (AAO) membranes and templates with a pore diameter of 200 nm were either purchased commercially (Anopore®, Whatman Inc.) or custom-made. The commercial AAO membranes contained open pores on both sides and are therefore referred to as "membrane" in the text. A back electrode of AuPd was sputtered on one side of the commercial membranes as a cathode using a tabletop sputterer (SC7640, Quorum Technologies). Prior to deposition, the backside of the AuPd electrode was isolated to ensure exclusive deposition inside the pores of the membrane and avoid deposition on the external surface of the back electrode.

The custom-made AAO templates (referred to as "template") contained self-ordered arrays of aligned cylindrical pores with narrow diameter distribution and are closed on one side. Self-ordered AAO was prepared by two-step anodization following procedures introduced by Masuda *et al.*[67] In the first step, an Al chip (Goodfellow, purity >99.999%) was anodized at 195 V for 10 h using 1 wt% H_3PO_3 cooled to 0–1 °C as the electrolyte solution. The resulting porous alumina layer was selectively removed by etching with an aqueous solution of 0.18 M CrO_3 and 0.72 M H_3PO_4. As a result, patterned Al substrates with hexagonal arrays of indentations were obtained. In the second step, hierarchical pores consisting of macroporous segments branching into dendritic mesopores were obtained by adapting a method introduced by Nielsch *et al.*[68] Using 1 wt% H_3PO_4 at 0–1 °C as the electrolyte solution, the anodization voltage $U(t)$ was directly reduced from 195 V to 80 V according to

$$U(t) = U_0 e^{-t/\tau}, \quad (5)$$

where U_0 is the start voltage of 195 V, τ is a constant, *i.e.* τ = 191.7 min in this case, and t is the anodization time (171 min to reach a voltage of 80 V). Then, the electrolyte was replaced by an aqueous solution of 0.3 M $C_2H_2O_4$, and the temperature was adjusted to 10 °C. Following the profile of eqn (5) with $U_0 = 80$ V and $\tau = 14.0$ min, the anodization voltage was further reduced to a target value of 0.01 V, which was reached after 125 min. Subsequently, the AAO layer was rinsed with deionized water. Prior to electrodeposition, the aluminium disks were isolated with nail varnish to ensure exclusive deposition inside the pores of these AAO templates.

The AAO membranes and templates were used as working electrodes in a three electrode setup, with a Pt sheet (Metrohm Autolab) as the counter electrode and Ag/AgCl in 3 M KCl (Metrohm Autolab) as the reference electrode. All potentials are given with respect to the reference electrode. These electrodes were connected to an Autolab PGSTAT 128N potentiostat. TiO_2 nanotubes were formed from an electrolyte containing 0.02 M $TiOSO_4$, 0.03 M H_2O_2, 0.05 M HNO_3 and 0.25 M KNO_3 with a pH of 1.4. Deposition occurred at −1.00 V for 6 h. After deposition, the gel was either dried overnight at 100 °C or annealed for 2 h at 650 °C in a tube furnace. Ag was electrodeposited for 15 min at +0.10 V in an aqueous electrolyte containing 0.20 M $AgNO_3$ and 0.10 M H_3BO_3 with pH adjusted to 1.5 using HNO_3. In the final steps, the nanowires or nanotubes were collected by dissolving the AAO membranes or templates in an aqueous solution of 1 M NaOH or in an aqueous solution of 0.18 M CrO_3 and 0.72 M H_3PO_4, respectively, followed by detachment from the back electrode by gentle swirling. In order to eliminate the NaOH or CrO_3 in the nanowire/nanotube solution, the solution was washed at least 5 times with water using a Hermle Z36HK centrifuge at 10 000 rpm for 5 min.

The TiO_2 nanotubes made by Atomic Layer Deposition (ALD) were also prepared inside custom-made AAO membranes with the same dimensions as the templates used for TiO_2 nanotube formation by the electrochemically induced sol–gel method. Amorphous TiO_2 was deposited at 120 °C using titanium(IV) isopropoxide preheated at 70 °C as the metal containing reactant and water vapor as the oxygen source. The porous membranes were coated using the exposure-mode sequence due to the high aspect ratio of these nanostructures, where a full ALD cycle consisted of 2 s pulse, 40 s exposure and 60 s purging for the titanium precursor, followed by 0.5 s pulse, 40 s exposure, and 60 s purging for the water vapor. Dried Ar was used as the carrier and purging gas and the process was carried out in a commercial ALD reactor SAVANNAH 100 (Cambridge NanoTech Inc., USA). After thermal annealing for 3 h at 400 °C and Au sputtering, Ag was electrodeposited at −1.2 V in a two-electrode setup using Pt as the counter electrode from an aqueous electrolyte containing 0.027 M Ag_2SO_4, 0.88 M diammonium citrate and 1.08 M KSCN at pH 4.5. The procedures used for dissolution of the AAO membrane and washing were the same as above.

Samples were measured with X-ray powder diffraction (XRD) to confirm the formation of crystalline TiO_2 phases in the membranes using a PANalytical X'Pert Pro (PANalytical B.V., Almelo, The Netherlands) instrument. Samples were measured from 2θ = 20–50°, with step sizes of 0.026° and 600 s per step using a PIXcel 1D scanning line detector. The spectra were further analyzed using the X'Pert Highscore Plus software package (version 3.0e). Scanning Electron Microscopy (SEM)

images were taken using a Zeiss HR-LEO 1550 FEG SEM or a Zeiss Merlin HRSEM. Transmission Electron Microscopy (TEM) images and Electron Energy Loss Spectroscopy (EELS) maps were taken with an Analytical TEM from FEI Instruments.

The photocatalytic activity of TiO_2 nanotubes with and without the Ag core was investigated by water splitting experiments in a custom-made setup consisting of 8 top-illuminated reactors with a volume of 36.4 mL each, connected to a Compact gas chromatograph (GC) (Interscience BV) equipped with a thermal conductivity detector (TCD). 5–14 mg of nanotubes/wires (1 completely filled AAO template with a diameter of ~3.5 cm) was dispersed in 15 mL of a 1 M NaOH stock solution (pH 13) that was bubbled with Ar gas for at least 30 min to remove a large part of the O_2 from the solution. Then the reactors were evacuated to 3 mbar and subsequently filled with Ar to remove all air from the head space in the reactors. After three evacuations, a 120 Watt high pressure Mercury lamp (Dr Gröbel UV-Elektronik GmbG) was turned on, of which the emission was divided over 12 optical fibers. During illumination, the formed H_2 was measured subsequently in each reactor. In a standard procedure, the composition in each reactor was measured every 15 min for 13 times. In a long-term measurement, the formed H_2 gas was measured 5 times using a measurement interval of 1.5 h.

Conclusions

The electrochemically induced sol–gel method was used to prepare anatase TiO_2 nanotubes in AAO membranes and templates with a diameter of 200 nm. By varying the intermediate thermal annealing process of the titania gel phase, the location where Ag deposited during the subsequent electrodeposition step in the same template could be tuned. Intermediate heating at 100 °C resulted in the formation of Ag nanoparticles incorporated in the shell of the TiO_2 nanotubes, while thermal annealing at 650 °C led to TiO_2 nanotubes filled with a continuous Ag phase, thus forming coaxial TiO_2–Ag nanowires. These coaxial TiO_2–Ag nanowires showed improved photocatalytic activity for direct water splitting due to the favorable geometry of core–shell systems, which is characterized by a large contact area between the photoactive material (TiO_2) and the H_2 evolution catalyst (Ag), photon reflection by the Ag core to capture the maximum number of photons in the titania phase, and short diffusion paths from the TiO_2 phase to the Ag phase in order to separate the exciton efficiently. During a long-term experiment, H_2 was formed at a rate of 1.2×10^{-3} mol g^{-1} h^{-1} for at least 6 h.

This technique is not only limited to the formation of TiO_2–Ag nanowires, but basically any combination of core–shell materials can be envisaged as long as electrodeposition or a related technique results in the formation of a nanotube for the shell material and a nanowire for the core material. Just as the choice of materials is not limited to what is described in this paper, also the possible applications are not limited to photocatalysis, but they can be extended to other areas, *e.g.* solar cells and batteries.

Acknowledgements

Financial support from the Chemical Sciences division of the Netherlands Organization for Scientific Research (NWO-CW) is gratefully acknowledged. Financial support from the center of excellence SFB 986 on Tailor-made Multi Scale Materials Systems funded by the German Science Foundation (DFG) is also gratefully acknowledged by JMMM and KN. C. Hess and H. Tobergte (University of Osnabrück) are gratefully acknowledged for the production of AAO templates used in this research; Chieh-Chao Yang and Rogier Besselink (University of Twente) are gratefully acknowledged for their help.

Notes and references

1 A. W. Maijenburg, E. J. B. Rodijk, M. G. Maas, M. Enculescu, D. H. A. Blank and J. E. ten Elshof, *Small*, 2011, **7**, 2709–2713.
2 Y. W. Heo, D. P. Norton, L. C. Tien, Y. Kwon, B. S. Kang, F. Ren, S. J. Pearton and J. R. Laroche, *Mater. Sci. Eng., R*, 2004, **47**, 1–47.
3 R. Fan, R. Karnik, M. Yue, D. Li, A. Majumdar and P. Yang, *Nano Lett.*, 2005, **5**, 1633–1637.
4 F. Patolsky, G. Zheng and C. M. Lieber, *Anal. Chem.*, 2006, **78**, 4260–4269.
5 C. D. Keating and M. J. Natan, *Adv. Mater.*, 2003, **15**, 451–454.
6 L. A. Bauer, D. H. Reich and G. J. Meyer, *Langmuir*, 2003, **19**, 7043–7048.
7 J. Wang, *J. Mater. Chem.*, 2008, **18**, 4017–4020.
8 W. F. Paxton, S. Sundararajan, T. E. Mallouk and A. Sen, *Angew. Chem., Int. Ed.*, 2006, **45**, 5420–5429.
9 Y. Wang, R. M. Hernandez, D. J. Bartlett Jr, J. M. Bingham, T. R. Kline, A. Sen and T. E. Mallouk, *Langmuir*, 2006, **22**, 10451–10456.
10 J. Wang, *ACS Nano*, 2009, **3**, 4–9.
11 T. S. Kang, A. P. Smith, B. E. Taylor and M. F. Durstock, *Nano Lett.*, 2009, **9**, 601–606.
12 M. Z. Hu, P. Lai, M. S. Bhuiyan, C. Tsouris, B. Gu, M. Parans Paranthaman, J. Gabitto and L. Harrison, *J. Mater. Sci.*, 2009, **44**, 2820–2827.
13 J. Jitputti, Y. Suzuki and S. Yoshikawa, *Catal. Commun.*, 2008, **9**, 1265–1271.
14 E. Y. Kim, J. H. Park and G. Y. Han, *J. Power Sources*, 2008, **184**, 284–287.
15 Y. Sun, G. Wang and K. Yan, *Int. J. Hydrogen Energy*, 2011, **36**, 15502–15508.
16 P. E. De Jongh, D. Vanmaekelbergh and J. J. Kelly, *J. Electrochem. Soc.*, 2000, **147**, 486–489.
17 C. J. Engel, T. A. Polson, J. R. Spado, J. M. Bell and A. Fillinger, *J. Electrochem. Soc.*, 2008, **155**, F37–F42.
18 S. Sunkara, V. K. Vendra, J. H. Kim, T. Druffel and M. K. Sunkara, *Catal. Today*, 2013, **199**, 27–35.
19 Z. Zhang, R. Dua, L. Zhang, H. Zhu, H. Zhang and P. Wang, *ACS Nano*, 2013, **7**, 1709–1717.
20 R. Van De Krol, Y. Liang and J. Schoonman, *J. Mater. Chem.*, 2008, **18**, 2311–2320.
21 A. Kudo and Y. Miseki, *Chem. Soc. Rev.*, 2009, **38**, 253–278.

22 T. Bak, J. Nowotny, M. Rekas and C. C. Sorrell, *Int. J. Hydrogen Energy*, 2002, **27**, 991–1022.
23 A. Fujishima and K. Honda, *Nature*, 1972, **238**, 37–38.
24 R. Abe, *J. Photochem. Photobiol., C*, 2010, **11**, 179–209.
25 P. Roy, D. Kim, K. Lee, E. Spiecker and P. Schmuki, *Nanoscale*, 2010, **2**, 45–59.
26 D. Eder, M. Motta and A. H. Windle, *Nanotechnology*, 2009, **20**, 055602.
27 C. J. Lin, Y. T. Lu, C. H. Hsieh and S. H. Chien, *Appl. Phys. Lett.*, 2009, **94**, 113102.
28 Y. Lin, S. Zhou, X. Liu, S. Sheehan and D. Wang, *J. Am. Chem. Soc.*, 2009, **131**, 2772–2773.
29 W. Nam and G. Y. Han, *J. Chem. Eng. Jpn.*, 2007, **40**, 266–269.
30 A. Wolcott, W. A. Smith, T. R. Kuykendall, Y. Zhao and J. Z. Zhang, *Small*, 2009, **5**, 104–111.
31 Y. Hong, M. Diaz, U. M. Córdova-Fteueroa and A. Sen, *Adv. Funct. Mater.*, 2010, **20**, 1568–1576.
32 M. G. Hosseini, M. M. Momeni and M. Faraji, *Electroanalysis*, 2010, **22**, 2620–2625.
33 L. Xing, J. Jia, Y. Wang, B. Zhang and S. Dong, *Int. J. Hydrogen Energy*, 2010, **35**, 12169–12173.
34 A. R. Armstrong, G. Armstrong, J. Canales and P. G. Bruce, *J. Power Sources*, 2005, **146**, 501–506.
35 B. L. He, B. Dong and H. L. Li, *Electrochem. Commun.*, 2007, **9**, 425–430.
36 C. M. Park, W. S. Chang, H. Jung, J. H. Kim and H. J. Sohn, *Electrochem. Commun.*, 2009, **11**, 2165–2168.
37 R. Yoshida, Y. Suzuki and S. Yoshikawa, *J. Solid State Chem.*, 2005, **178**, 2179–2185.
38 S. P. Albu, A. Ghicov, S. Berger, H. Jha and P. Schmuki, *Electrochem. Commun.*, 2010, **12**, 1352–1355.
39 W. Jun and L. Zhiqun, *J. Phys. Chem. C*, 2009, **113**, 4026–4030.
40 S. Li, G. Zhang, D. Guo, L. Yu and W. Zhang, *J. Phys. Chem. C*, 2009, **113**, 12759–12765.
41 M. S. Sander, M. J. Côté, W. Gu, B. M. Kile and C. P. Tripp, *Adv. Mater.*, 2004, **16**, 2052–2057.
42 C. Bae, Y. Yoon, H. Yoo, D. Han, J. Cho, B. H. Lee, M. M. Sung, M. Lee, J. Kim and H. Shin, *Chem. Mater.*, 2009, **21**, 2574–2576.
43 S. Inoue, S. Z. Chu, K. Wada, D. Li and H. Haneda, *Sci. Technol. Adv. Mater.*, 2003, **4**, 269–276.
44 Z. Ye, H. Liu, I. Schultz, W. Wu, D. G. Naugle and I. Lyuksyutov, *Nanotechnology*, 2008, **19**, 325303.
45 S. J. Limmer, S. Seraji, Y. Wu, T. P. Chou, C. Nguyen and G. Z. Cao, *Adv. Funct. Mater.*, 2002, **12**, 59–64.
46 Y. Lin, G. S. Wu, X. Y. Yuan, T. Xie and L. D. Zhang, *J. Phys.: Condens. Matter*, 2003, **15**, 2917–2922.
47 S. Liu and K. Huang, *Sol. Energy Mater. Sol. Cells*, 2005, **85**, 125–131.
48 X. Y. Zhang, L. D. Zhang, W. Chen, G. W. Meng, M. J. Zheng, L. X. Zhao and F. Phillipp, *Chem. Mater.*, 2001, **13**, 2511–2515.
49 Z. Miao, D. Xu, J. Ouyang, G. Guo, X. Zhao and Y. Tang, *Nano Lett.*, 2002, **2**, 717–720.
50 X. J. Wu, F. Zhu, C. Mu, Y. Liang, L. Xu, Q. Chen, R. Chen and D. Xu, *Coord. Chem. Rev.*, 2010, **254**, 1135–1150.
51 J. M. Macak, B. G. Gong, M. Hueppe and P. Schmuki, *Adv. Mater.*, 2007, **19**, 3027–3031.
52 C. Natarajan and G. Nogami, *J. Electrochem. Soc.*, 1996, **143**, 1547–1550.
53 S. Karuppuchamy, D. P. Amalnerkar, K. Yamaguchi, T. Yoshida, T. Sugiura and H. Minoura, *Chem. Lett.*, 2001, 78–79.
54 S. Karuppuchamy, K. Nonomura, T. Yoshida, T. Sugiura and H. Minoura, *Solid State Ionics*, 2002, **151**, 19–27.
55 S. A. Kumar, P. H. Lo and S. M. Chen, *Nanotechnology*, 2008, **19**, 255501.
56 M. G. Maas, E. J. B. Rodijk, W. Maijenburg, J. E. ten Elshof and D. H. A. Blank, in *Multifunction at the Nanoscale through Nanowires*, ed. K. Nielsch, A. Fontcuberta, I. Morral, J. K. Holt and C. V. Thompson, Materials Research Society, Pittsburg, 2010, pp. M01–08.
57 J. Sekulić, J. E. ten Elshof and D. H. A. Blank, *Adv. Mater.*, 2004, **16**, 1546–1550.
58 V. Lyahovitskaya, Y. Feldman, I. Zon, A. Yoffe and A. I. Frenkel, *J. Mater. Res.*, 2012, **27**, 2819–2828.
59 A. Di Paola, G. Cufalo, M. Addamo, M. Bellardita, R. Campostrini, M. Ischia, R. Ceccato and L. Palmisano, *Colloids Surf., A*, 2008, **317**, 366–376.
60 A. M. Luís, M. C. Neves, M. H. Mendonça and O. C. Monteiro, *Mater. Chem. Phys.*, 2011, **125**, 20–25.
61 C. A. Grimes and G. K. Mor, in *TiO_2 nanotube arrays: Synthesis, properties and applications*, Springer, *Dordrecht Heidelberg London New York*, 2009, pp. 149–216.
62 M. Kim, C. Bae, H. Kim, H. Yoo, J. M. Montero Moreno, H. S. Jung, J. Bachmann, K. Nielsch and H. Shin, *J. Mater. Chem. A*, 2013, **1**, 14080–14088.
63 J. A. Seabold and K. S. Choi, *J. Am. Chem. Soc.*, 2012, **134**, 2186–2192.
64 R. Abe, K. Sayama and H. Arakawa, *Chem. Phys. Lett.*, 2003, **371**, 360–364.
65 R. Abe, K. Sayama, K. Domen and H. Arakawa, *Chem. Phys. Lett.*, 2001, **344**, 339–344.
66 K. Lee, W. S. Nam and G. Y. Han, *Int. J. Hydrogen Energy*, 2004, **29**, 1343–1347.
67 H. Masuda, K. Yada and A. Osaka, *Jpn. J. Appl. Phys., Part 2*, 1998, **37**, L1340–L1342.
68 K. Nielsch, F. Müller, A. P. Li and U. Gösele, *Adv. Mater.*, 2000, **12**, 582–586.